THE JOURNAL OF PHYSICAL CHEMISTRY B

ARTICLE

pubs.acs.org/JPCB

Binding Site Influence on the Electronic Structure and Electron Paramagnetic Resonance Properties of the Phyllosemiquinone Free Radical of Photosystem I

Tzu-Jen Lin and Patrick J. O'Malley*

School of Chemistry, The University of Manchester, Manchester M13 9PL, U.K.

Supporting Information

ABSTRACT: Electronic structure calculations are performed on models of the phyllosemiquinone (PhSQ) free radical in the A_{1A} and A_{1B} sites of photosystem I. Partial geometry optimization of each site is performed, and from the resultant geometry spin densities and hyperfine couplings are calculated. We exploit the ONIOM methodology to progressively build up a model of the A_{1A} site and monitor the effect on the spin density distribution of the PhSQ and its hyperfine couplings. For the A_{1A} site, we show that while the O1 atom of the PhSQ is not involved in direct hydrogen bonding, the ^{17}O anisotropic hyperfine coupling for this position is sensitive to interactions with neighboring groups, especially Trp A697 and Phe A689. The results obtained are in agreement with experimental determinations which indicate small differences in ^{17}O hyperfine couplings for both oxygen atoms. Good agreement between calculated and experimental ^{1}H and ^{13}C hyperfine couplings is also found. In addition, we find that a significant ^{14}N isotropic coupling of 1.4 MHz is calculated for the peptide NH group of Leu A722. The ^{14}N isotropic hyperfine coupling obtained for the indole nitrogen atom of Trp A697 is calculated to be zero in disagreement with a previous experimental assignment. The spin density distribution of the PhSQ in the A_{1B} site is calculated to be very similar to that in the A_{1A} site. The presence of just one relatively weak hydrogen bond to the photosytem I quinone is proposed to contribute substantially to its relatively low redox potential when compared with the more strongly hydrogen bonded quinone acceptors present in type II reaction centers.

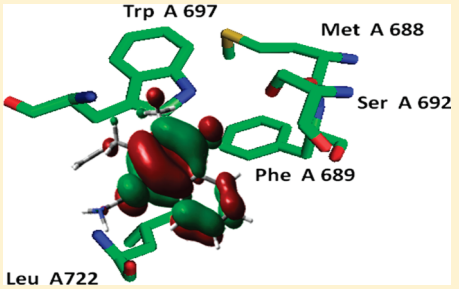

INTRODUCTION

Solar energy conversion in photosynthesis begins with the primary process of light-induced charge separation in reaction centers (RCs). The RCs are membrane-bound protein complexes which contain the cofactor pigment molecules chlorophyll, pheophytin, and quinone involved in charge separation. In cyanobacteria, algae, and higher plants, two RCs, photosystem I (PS I) and photosystem II (PS II), function with similar cofactor pigments enabling electrons to be transferred from water to ferredoxin.[1] PS I from the cyanobacterium *Thermosynechococcus elongates* was crystallized, and an X-ray crystallographic structure at 2.5 Å has been obtained.[2] The cofactors of the electron transport chain are arranged in two branches A and B as pairs of molecules related by a pseudo-C2 axis (Figure 1). The nature and kinetics of the primary steps in charge separation are a controversial topic of discussion.[3] Recently, it was proposed that $P700^{\bullet+}$ is generated only after oxidation of the accessory Chl molecules (A_A and A_B; see Figure 1). The first stable intermediate, P700 $^{\bullet+}A_0^{\bullet-}$, is generated within a few picoseconds after light excitation. The next electron acceptor A_1 (phylloquinone) is reached in~30 ps. Then, the electron is transferred to F_X, which is a [4Fe−4S] cluster bound to PsaA and PsaB. The PsaC-bound [4Fe−4S] clusters F_A and F_B follow in the electron transfer chain. In less than 1 ms, the electron reaches the terminal electron acceptor F_B, located on the stromal side. It is currently believed that both pigment branches are actively involved in electron transfer at physiological temperatures although the exact role of each pathway is still a matter of some discussion.[4−6]

Electron paramagnetic resonance (EPR) methods have been some of the major tools in the investigation of the radicals created during photosynthetic electron transfer.[7] In particular, hyperfine couplings measured using EPR, ENDOR, and ESEEM methods can be used to provide a measure of the unpaired spin density distribution of the free radicals involved. Perturbation of the spin density distribution of the free radicals caused by their interaction with the protein matrix can be monitored and has led to significant insight into the nature of such interactions. As these interactions are key factors in adjusting the redox potential of the electron transfer cofactors, such knowledge is indispensable in elucidating the role of the protein matrix in tuning the cofactors to perform their function. Assignment of hyperfine couplings to molecular positions can be problematic as the spectra are usually powderlike and isotopic substitution is limited. The assignment problem has been aided considerably in recent years by the

Received: April 14, 2011
Revised: June 3, 2011
Published: June 12, 2011

ACS Publications © 2011 American Chemical Society

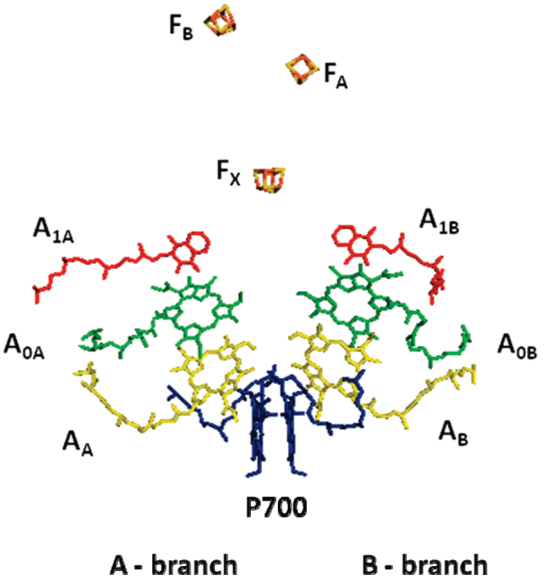

Figure 1. Arrangement of the cofactors in the electron transport chain of PS I showing the two branches A and B along which electron transfer occurs from P700 to ferredoxin. See the text for a description of initial electron transfer events.

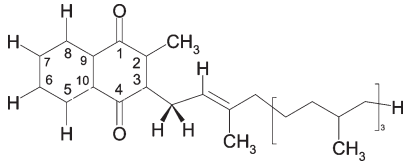

Figure 2. Phylloquinone (PhQ) molecular structure and numbering scheme.

performance of parallel density functional theory (DFT) calculations which provide very accurate spin density distributions and hyperfine couplings for chlorophyll and semiquinone free radical models.[8] In addition, these calculations allow a unique insight into the electronic structure properties of the pigments involved and extended models are being increasingly used to model the interactions of the pigments with the protein matrix.[9]

In this paper we focus on electronic structure modeling of the PS I A_1 acceptor, a phylloquinone (PhQ) molecule (Figure 2). The quinone sites present in the two electron transfer chains are denoted A_{1A} and A_{1B}. The X-ray crystal structure indicates identical environments for both quinones (Figure 3). After the initial confirmation of the A_1 radical as a phyllosemiquinone (PhSQ),[10] it was noted that the strong ENDOR signal corresponding to the ^{1}H hyperfine coupling of the 2-CH_3 group had an increased value compared with the radical generated in alcohol solvents.[11] No explanation was given for this at the time, and it was hypothesized that this arose from π stacking with a neighboring Trp residue.[12] Using DFT calculations on model systems, O'Malley[13] proposed that this elevated 2-CH_3 ^{1}H hyperfine coupling arose from an asymmetric spin density distribution for the PhSQ in its binding site caused by hydrogen bonding to the O4 oxygen atom only. The crystal structure determination of Jordan et al.[2] showed that, for PhQ in the A_{1A} and A_{1B} sites, only single-sided hydrogen bonding from the peptide NH groups of Leu A722 and Leu B706 to the O4 atom

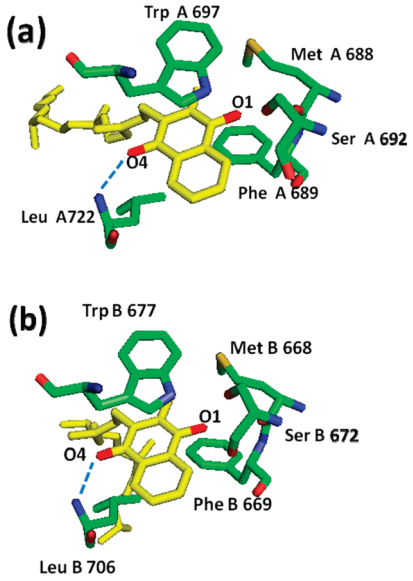

Figure 3. (a) A_{1A} and (b) A_{1B} sites, illustrating PhQ in yellow and nearest neighbor amino acids. The putative hydrogen bond between the O4 atom of the PhQ and the peptide NH of both Leu A722 and Leu B706 is illustrated by the dashed blue line.

existed in both sites (Figure 3). No hydrogen bonding to the O1 atom was evident. Subsequent EPR studies confirmed that, for the PhSQ radical in the A_{1A} site, hydrogen bonding to only O4 exists[4,14−18] and this leads to an asymmetric spin density distribution as originally proposed in ref 13. An additional interesting and related feature of PS I is the relatively low redox potential of the quinone in both sites compared with the quinone in aqueous or alcohol solution.[4,10] In addition, it has been shown that quinones present in the A_1 site have significantly lower redox potentials (>600 mV) compared with identical quinones present in the Q_A site of PS II.[16,19] This large difference arises from specific protein interactions in both binding sites which alter the stability of the semiquinone form compared with the alcohol and aqueous solution. For one-electron quinone reduction to the semiquinone form, hydrogen bonding stabilizes the semiquinone form, increasing the redox potential of the quinone. The increase in redox potential brought about by hydrogen bonding depends on the both the number and strength of the hydrogen bonds formed.[13,20,21]

In this paper our own *N*-layered integrated molecular orbital and molecular mechanics (ONIOM)[22] calculations are performed on models of the A_{1A} and A_{1B} sites containing the PhSQ radical. Partial geometry optimization of each site is performed, and from the resultant geometry spin densities and hyperfine couplings are calculated. We focus on the A_{1A} site PhSQ as this is the semiquinone characterized by EPR methods.[15] We exploit the ONIOM methodology to progressively build up a model of the A_{1A} site and monitor the effect on the spin density distribution of the PhSQ and its hyperfine couplings. We show that while the O1 atom of the PhSQ is not involved in direct hydrogen bonding, the ^{17}O anisotropic hyperfine coupling for this position is sensitive to interactions with neighboring groups, leading to a lowering in the magnitude of the anisotropic hyperfine coupling. The resulting lower asymmetries in the O1 and O4 ^{17}O hyperfine couplings are in agreement with experimental determinations which indicate small differences in ^{17}O hyperfine coupling magnitudes for both

Table 1. Optimized PhSQ Geometries[a]

	isolated	A_{1A}	A_{1B}
C1−O1	1.264	1.259	1.259
C4−O4	1.265	1.283	1.285
O4−H		1.644	1.707

[a] Isolated PhSQ was geometry optimized at the B3LYP/6-31G(d) level. All distances are in angstroms.

PhSQ oxygen atoms.[23] Smaller models used so far, which ignore any O1 interactions, are unable to reproduce these experimental findings. Good agreement between calculated and experimental ^{1}H and ^{13}C hyperfine couplings is also found. In addition, for our extended site models, we find that a significant ^{14}N isotropic coupling is calculated for the peptide NH group of Leu A722. The ^{14}N isotropic hyperfine coupling obtained for the indole nitrogen atom of Trp A697 is calculated to be zero in disagreement with a previous experimental assignment. The spin density distribution of the PhSQ in the A_{1B} site is shown to be very similar to the A_{1A} site.

METHODS

Starting with the PS I structure of Jordan et al.[2] (PDB entry, 1JB0), we created a model of the A_{1A} and A_{1B} sites. For A_{1A}, the model consisted of PhSQ and residues Phe A685 to Leu A700 and Arg A720 to Ile A725. For A_{1B}, PhSQ and residues Thr B665 to Val B685 and Pro B703 to Ser B720 were included. Hydrogens were added and the phylloquinone isoprene chain was reduced to CH2CHCH2. For optimization studies, two-layer ONIOM calculations ONIOM(B3LYP/6-31G(d):UFF) were performed. For the A_{1A} site, the QM layer contained the phyllosemiquinone, Leu A722, Trp A697, Phe A689, Ser A692, and Met A688; see Figure 3a. For the A_{1B} site the QM layer contained PhSQ, Trp B677, Phe B669, Ser B672, Met B668, and Leu B706. The remaining atoms of the protein site formed the MM layer. Linking between the QM and MM layers was achieved using hydrogen link atoms. Charges for the MM layer were generated using the qEq method and electrostatic embedding; i.e., ONIOM-EE was employed.[24] Keeping all heavy (non-hydrogen) atoms except the PhSQ fixed, we optimized the PhSQ geometry within both sites. This geometry was then used in all single point ONIOM(B3LYP/EPR-II:UFF) calculations to obtain spin densities and hyperfine couplings. As only atoms in the QM layer will contribute to spin density and hyperfine couplings, by moving atoms between the QM and MM layer we can either include or exclude atoms from influencing the spin density distribution and resultant hyperfine couplings of the PhSQ. In such a fashion we exploit the ONIOM layering method to develop a strategy for progressively building up the environment around the PhSQ whereby the direct influence of specific residues in the quinone binding site on its spin density distribution can be assessed. Using this procedure, the models studied were the following:

model A: PhSQ isolated
model B: model A plus Leu A722
model C: model B plus Trp A697
model D: model C plus Ser A692
model E: model D plus Phe A689
model F: model E plus Met A688

All of the above calculations were performed using mechanical embedding. All calculations were performed using Gaussian 09.[24]

RESULTS AND DISCUSSION

Geometry. The CO and H bond lengths obtained for optimized PhSQ isolated and in the A_{1A} and A_{1B} sites are given in Table 1. Minute differences are found for both radicals. The H-bond from the peptide NH of Leu A722/B706 to the O4 oxygen of the PhSQ is calculated to be slightly longer for A_{1B} by 0.05 Å. In both cases the optimized C4O4 bond length has increased in the binding site by 0.02 Å compared with the isolated free radical. This can be attributed to hydrogen bond formation at this oxygen atom. As mentioned in the Introduction, the original DFT calculations in ref 13 were the first to invoke one-sided hydrogen bonding to the A_1 semiquinone. This was confirmed by the crystal structure determination for PS I which showed hydrogen bonding of PhQ to the O4 only via hydrogen bond donation from the Leu A722/B706 peptide NH group (Figure 3). No hydrogen bonding was in evidence to the O1 atom. Our optimization of the PhSQ in the A_{1A} and A_{1B} sites above indicates that a similar situation arises for the PhSQ with hydrogen bonding to O4 only and no hydrogen bond in evidence to O1. For the A_{1A} site potential hydrogen bond donors to O1 such as the Ser A692 OH group are calculated to be 3.1 Å away. Instead, this residue is involved in hydrogen bond donation to the peptide carbonyl of Met A688. Another potential hydrogen bond donor is the Nε group of Trp A697, but this is calculated to be 3.3 Å from O1 and is not suitably oriented for hydrogen bond formation. From the calculated structure this NH group acts as a hydrogen bond donor to the OH group of Ser A692. An identical pattern is found for the A_{1B} site.

^{17}O and ^{13}C Hyperfine Couplings. For the A_{1A} site PhSQ, single point calculations were performed on models A−F to obtain spin densities and hyperfine couplings. The ^{17}O and ^{13}C anisotropic hyperfine couplings obtained for the C1, C4, O1, and O4 positions are given in Table 2. As demonstrated previously,[25] the magnitudes of these hyperfine couplings are a direct measure of the spin density at these atom positions within the radical. When added to the isotropic component, also given in Table 2, they give overall hyperfine couplings which can be compared with experimental measurements. In the following we concentrate our analysis on the largest T_{33} component. Model A contains the PhSQ in the QM layer and therefore reflects the spin density distribution of the "free" PhSQ without any neighboring interactions. Model B is similar to the model used in the original study of ref 13 with an H-bond to the O4 atom from the peptide NH group of Leu A722 included in the QM layer. The changes in spin population and hyperfine couplings are very similar to those in our earlier report[13] which were also reproduced in ref 15 more recently. As shown in these previous studies, this small model, taking into account only the H-bond to O4, can account well for the observed ^{1}H hyperfine couplings measured. The H-bond to O4 gives rise to an odd alternant spin density distribution around the PhSQ ring with raised spin density occurring at C4, C2, and O1 while the O4, C1, and C3 spin density values are lowered compared with the isolated radical. This model originally explained[13] the raised spin density at the C2 position as revealed experimentally by an increased value for the 2-CH_3 ^{1}H hyperfine coupling compared with the radical generated in alcohol solvents.[26]

^{1}H hyperfine couplings, for all ring positions, recently obtained from high resolution ENDOR and TRIPLE studies show good agreement with DFT calculations on this model.[15] The major disagreement with experiment occurs for the comparison

Table 2. Calculated PhSQ, ^{13}C and ^{17}O Anisotropic (T_{nn}) and Isotropic (A_{iso}) Hyperfine Coupling Values, for A_{1A} Site Models[a]

position	T_{nn}, A_{iso}	model A	model B	model C	model D	model E	model F
O1	T_{11}	37.6	37.4	35.2	34.6	33.2	33.2
	T_{22}	36.9	36.9	34.7	34.1	32.7	32.6
	T_{33}	**−74.5**	**−74.3**	**−69.9**	**−68.7**	**−65.9**	**−65.8**
	A_{iso}	−19.3	−18.5	−17.5	−17.4	−16.9	−17.4
O4	T_{11}	35.5	31.3	31.5	31.4	31.3	31.8
	T_{22}	34.9	30.6	30.8	30.7	30.6	31.0
	T_{33}	**−70.4**	**−62.0**	**−62.3**	**−62.1**	**−62.0**	**−62.8**
	A_{iso}	−18.1	−17.5	−17.4	−17.3	−17.2	−17.5
C1	T_{11}	−9.8	−8.0	−9.4	−9.7	−10.8	−10.5
	T_{22}	−6.3	−4.3	−6.0	−6.3	−7.7	−7.4
	T_{33}	**16.1**	**12.3**	**15.3**	**16.0**	**18.4**	**17.9**
	A_{iso}	−6.8	−10.6	−8.0	−7.4	−5.4	−5.5
C4	T_{11}	−10.1	−15.8	−15.4	−15.5	−15.2	−15.0
	T_{22}	−6.5	−13.4	−12.9	−13.0	−12.8	−12.5
	T_{33}	**16.6**	**29.1**	**28.4**	**28.4**	**28.0**	**27.6**
	A_{iso}	−6.2	4.5	3.8	3.8	3.4	3.0

[a] All values are given in MHz. T_{33} values discussed in the text are highlighted in bold.

Table 3. Calculated PhSQ, ^{13}C and ^{1}H Anisotropic (T_{nn}) and Isotropic (A_{iso}) Hyperfine Coupling Values, for A_{1A} Site Models[a]

position	T_{nn}, A_{iso}	model A	model B	model C	model D	model E	model F
C2	T_{11}	−9.5	−13.0	−11.4	−11.4	−11.2	−10.7
	T_{22}	−9.0	−12.7	−11.1	−11.2	−10.9	−10.4
	T_{33}	18.6	25.3	22.5	22.6	22.1	21.1
	A_{iso}	2.2	8.7	6.5	6.3	5.4	5.1
^{1}H, CH_3(2)	A_{iso}	7.7	10.9	9.7	9.6	9.5	9.4

[a] All values are given in MHz.

with measured ^{17}O hyperfine couplings.[23] Table 2 shows that the calculated isotropic values for O1 and O4 differ by 1 MHz while the T_{33} anisotropic values differ by 12.3 MHz. The total (isotropic plus anisotropic) A_{33} component is therefore predicted to possess a difference of 13.3 MHz for O1 and O4. This is similar to previous reports.[13,15] The experimentally determined difference[23] is 7 MHz, around half the calculated value. The experimental value is also in striking contrast to the approximately 19 MHz difference measured for the ubisemiquinone (USQ) radical in the bRC of *Rhodobacter sphaeroides*.[7] In order to explain the small difference in ^{17}O hyperfine couplings for PhSQ in the A_1 site, it was claimed[23] that this hyperfine coupling is not a sensitive measure of the spin density on the oxygen atom. While this is partially true for the isotropic part,[21] it is incorrect for the anisotropic contribution which is actually the most direct measure of the spin density on the oxygen atom.

As the crystal structure showed no hydrogen bonding interactions with the O1 atom of the PhQ in both A_1 sites, modeling studies used after the crystal structure determination have only included the H-bond to the O4 atom; it has been assumed that other interactions within the site do not affect the PhSQ spin density distribution. Because of the larger model of the A_1 site used in this study we can test this assumption. To do this, as explained in the Methods section, we have used the ONIOM layering procedure to gradually include nearby amino acids of the A_{1A} binding site into the QM layer, thereby allowing us to assess their influence on the spin density distribution of the PhSQ residing there. In model C we extend model B by introducing the Trp A697 ring into the QM layer. Table 2 shows that including this interaction in the QM region leads to a significant reduction in the magnitude of the O1 anisotropic hyperfine coupling, reducing the principal T_{33} magnitude by 4.4 MHz. The O4 value is left essentially unchanged. In model D we add in the Ser A692 OH interaction. Compared with model C the T_{33} O1 anisotropic hyperfine coupling magnitude is reduced by a further 1.2 MHz, suggesting a weak interaction between O1 and the Ser OH group. In model E we include Phe A689. Including this interaction in our QM model leads to a reduction of another 3.8 MHz in the magnitude of the O1 value. Further extension to Met A688, model F, does not lead to any significant changes in hyperfine couplings measured. It is clear therefore that inclusion of regions of the A_{1A} site near the O1 atom in the QM layer do lead to a significant reduction in its ^{17}O anisotropic hyperfine coupling magnitude while having no effect on the O4 value. This lowers the observed asymmetry between the O1 and O4 atoms in agreement with the experimental observation.[23] While no direct H-bonding occurs to the O1 atom in the A_{1A} site, we show that including these nearest-neighbor groups leads to a significant lowering of the O1 spin density value as reflected in the reduced anisotropic hyperfine coupling value. As has been previously shown, the effect of H-bonding on semiquinone spin density is to effectively transfer spin density from the O atom to the C atom of the carbonyl group.[25] This is clearly demonstrated by the hydrogen bond from the Leu A722 NH group in this study (model A); see Table 2. We note from Table 2 that including extra interactions near O1 (models B−F) leads to a lowering in

Table 4. Calculated ^{1}H and ^{14}N Hyperfine Couplings for the Peptide NH Group of Leu A722 and the Indole NH group of Trp A697 for Models B, D, E, and F[a]

		model B	model D	model E	model F
Trp A697 (ring NH)					
^{1}H	A_{iso}		0.0	0.0	−0.1
	T_{11}		−1.5	−1.5	−1.5
	T_{22}		−0.8	−0.8	−0.8
	T_{33}		2.3	2.3	2.3
^{14}N	A_{iso}		−0.1	0.0	0.0
	T_{11}		−0.2	−0.2	−0.2
	T_{22}		−0.1	−0.2	−0.1
	T_{33}		0.3	0.3	0.3
	NQCC		3.3	3.3	3.3
	η		0.3	0.3	0.3
Leu A722 (peptide NH)					
^{1}H	A_{iso}	−1.1	−1.2	−1.2	−0.9
	T_{11}	−5.1	−5.1	−5.1	−5.0
	T_{22}	−4.7	−4.7	−4.8	−4.7
	T_{33}	9.8	9.8	9.9	9.7
^{14}N	A_{iso}	1.4	1.4	1.4	1.4
	T_{11}	−0.3	−0.3	−0.3	−0.2
	T_{22}	−0.2	−0.2	−0.2	−0.2
	T_{33}	0.5	0.5	0.5	0.5
	NQCC		3.8	3.8	3.9
	η		0.7	0.7	0.7

[a] Calculated values for the nuclear quadrupole coupling constant (NQCC) and the asymmetry parameter, η, are also given. All values except η are given in MHz.

the magnitude of the O1 anisotropic hyperfine coupling equivalent to that brought about by a single H-bond to the O4 atom. The significantly increased anisotropic hyperfine coupling of C4 is not observed for C1; however, the lowering in the spin density of O1 is accompanied by a lower increased spin density on C1. While the residues referred to above are obviously not in hydrogen bond contact with the O1 atom of PhSQ, it is likely that the spin density changes are brought about by weak dipolar interactions between certain groups in these residues and the O1 atom. Interactions with the α-CH group of Phe A689 and the indole NH group of Trp A697 are particularly significant as both groups exhibit significant ^{1}H anisotropic hyperfine couplings; see below.

It should also be noted that there are small changes to the C2 spin density value with model size (Table 3). This is to be expected from spin polarization arguments where the increased spin density on C1 with extended models will lead via spin polarization to a slightly lower C2 spin density value. Significantly, this is reflected in a change in the calculated $^{1}H-CH_3(2)$ hyperfine coupling constant (Table 3). The main manifestation of this change is apparent in going from model B to model C, where inclusion of the Trp A697 indole ring (model C) reduces the calculated 2-CH_3 ^{1}H isotropic hyperfine coupling from 10.9 to 9.7 MHz. Experimental ENDOR data[27] for a TrpA697Phe mutant reveals an increase in this hyperfine coupling of around 0.7 MHz compared with the wild type, i.e., in qualitative accord with the calculated trend.

As mentioned previously, the situation in PS I contrasts with the situation in bacterial type II RCs, where a much larger

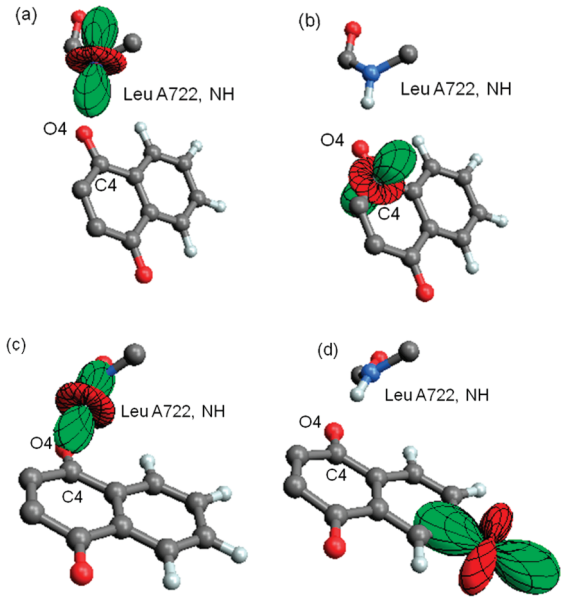

Figure 4. Polar plot representation of the anisotropic hyperfine coupling tensor for (a) the peptide N nucleus of Leu A722 (b) the C4 nucleus, (c) the peptide H nucleus of Leu A722, and (d) the H7 nucleus. The tensor is plotted as a surface showing the sign and symmetry visually, with red representing negative values and green representing positive values. All values are scaled to facilitate viewing. See the text and ref 36 for further details of this type of representation.

difference of 19 MHz is observed experimentally between the O1 and O4 A_{33} hyperfine coupling for the oxygen atoms of the ubisemiquinone.[7] In the type II reaction centers hydrogen bonds to both O1 and O4 atoms are present.[28,29] Crucially, the experimental asymmetry can be reproduced by DFT calculations on extended models of the bacterial reaction center site and has been shown to be mainly attributable to the very strong hydrogen bond formed between the O4 oxygen atom and the δNH group of the His M219 residue.[9] His M219 is also a ligand to the non-heme Fe^{2+} or other divalent ions substituted there such as Zn^{2+}. This leads to a significant strengthening of the hydrogen bond formed to the O4 of the ubisemiquinone. In the A_{1A} site of PS I, the hydrogen bond formed by O4 and the peptide NH group of Leu A722 is much weaker. This can be gauged from the decrease in the O4 T_{33} component arising from hydrogen bonding . In the A_{1A} site the hydrogen bond to O4, of model B, brings about a reduction of 8.4 MHz in the T_{33} magnitude compared with the isolated radical (Table 2). For the Q_A site in *Rba. sphaeroides* the interaction with the Zn^{2+} ligated His M219 leads to a reduction in the O4 T_{33} magnitude of 21.4 MHz using the same theory level.[9] These findings suggest that the hydrogen bond strength in type II reaction centers is much stronger than that undergone by the PhSQ in the A_1 site of PS I. This difference in hydrogen bond strength and number will be a major contributing factor to the difference in redox potential of >600 mV observed for the PS I and PS II quinone binding sites.[4]

^{14}N Hyperfine Couplings. A novel feature of semiquinones in photosynthetic reaction centers has been the detection of ^{14}N hyperfine couplings caused by spin density delocalization from the SQ onto neighboring amino acid residues. These have been detected using ESEEM for the SQ in *Rba. sphaeroides*, photosystem II and photosystem I.[30−34] The ability of DFT methods to accurately model these interactions has been demonstrated

Table 5. ^{1}H Isotropic (A_{iso}) and Anisotropic (T_{nn}) Hyperfine Couplings Calculated for the A_{1A} and A_{1B} Sites[a]

	A_{1A}			A_{1B}		
	T_{33}	A_{iso}	A_{33}	T_{33}	A_{iso}	A_{33}
	T_{22}		A_{22}	T_{22}		A_{22}
position	T_{11}		A_{11}	T_{11}		A_{11}
H2	2.8	9.2	12.0 (12.4)	2.8	9.7	12.5
	−0.9		8.3 (8.3)	−0.9		8.8
	−1.9		7.3 (8.8)	−1.9		7.8
H3a	2.1	3.6	5.7	2.0	3.2	5.2
	−0.5		3.1	−0.5		2.7
	−1.4		2.2	−1.4		1.8
H3b	3.8	0.4	4.2	3.6	0.3	3.9
	−1.3		−0.9	−1.2		−0.9
	−2.5		−2.1	−2.4		−2.1
H5	2.1	−1.3	0.8 (−0.3)	2.5	−1.1	1.4
	−0.2		−1.5 (−1.9)	−0.8		−1.9
	−1.9		−3.2 (−3.6)	−1.6		−2.7
H6	1.9	−1.6	0.3 (0.5)	2.1	−1.7	0.4
	−0.7		−2.3 (−2.1)	−0.3		−2.0
	−1.2		−2.8 (−1.1)	−1.8		−3.5
H7	2.5	−2.9	−0.4 (−0.7)	1.9	−2.7	−0.8
	−0.6		−3.5 (−3.5)	−0.6		−3.3
	−1.9		−4.8 (−5.0)	−1.3		−4.0
H8	2.6	−0.1	2.5 (3.5)	2.3	−0.1	2.2
	−0.7		−0.8 (−0.8)	−0.6		−0.7
	−1.9		−2.0 (−1.3)	−1.7		−1.8
H (peptide NH) (Leu A722/Leu B706)	9.7	−0.9	8.8 (7.4)	9.9	−1.2	8.7
	−4.7		−5.6 (−3.5)	−4.8		−6.0
	−5.0		−5.9 (−3.5)	−5.1		−6.3

[a] For the 2-CH_3 group the average value for the three protons is given. The total (A_{nn}) values are also given for the A_{1A} site, where they are compared with the most recent experimental determinations[15] given in parentheses. All values are given in MHz.

Table 6. ^{13}C Isotropic (A_{iso}) and Anisotropic (T_{nn}) Hyperfine Couplings Calculated for the A_{1A} and A_{1B} Sites[a]

	A_{1A}			A_{1B}		
	T_{11}	A_{iso}	A_{11}	T_{11}	A_{iso}	A_{11}
	T_{22}		A_{22}	T_{22}		A_{22}
position	T_{33}		A_{33}	T_{33}		A_{33}
C1	−10.5	−5.5	−16.0 (15)	−9.9	−7.1	−17.0
	−7.4		−12.9 (15)	−6.5		−13.6
	17.9		12.4 (8)	16.4		9.3
C2	−10.7	5.1	−5.6	−11.2	5.6	−5.6
	−10.4		−5.3	−10.8		−5.2
	21.1		26.2	22.0		27.6
C3	−5.6	−5.4	−11.0	−4.5	−5.5	−10.0
	−4.9		−10.3	−3.8		−9.3
	10.4		−5.0	8.3		2.8
C4	−15.0	3.0	−12.0 (10.5)	−14.3	2.2	−12.1
	−12.5		−9.5 (10.5)	−11.7		−9.5
	27.6		30.6 (40)	26.1		28.3
C5	−1.3	−1.5	−2.8	−1.0	−1.7	−2.7
	0.2		−1.3	0.0		−1.7
	1.4		−0.1	1.0		−0.7

[a] The total, A_{nn}, values are also given for the C1 and C4 positions in the A_{1A} site, where they are compared with experimental magnitude determinations given[17] in parentheses. All values are given in MHz.

with impressive agreement between calculated and experimental values for *Rba. sphaeroides*.[9,33] Table 4 shows the calculated ^{14}N values for the peptide NH of Leu A722 and the indole ring N of Trp A697 together with the ^{1}H isotropic and anisotropic values. The calculated isotropic ^{14}N hyperfine coupling value is zero for the Trp A697 indole N atom. By contrast, a significant ^{14}N isotropic hyperfine coupling value of 1.4 MHz is calculated for the Leu A722 peptide NH group which is hydrogen bonded to the O4 atom of the PhSQ. Large anisotropic ^{1}H values are also calculated for the Leu A722 peptide NH interaction in contrast to the smaller values calculated for the indole NH group of Trp A697. The data in Table 3 suggest that the large ^{14}N isotropic hyperfine coupling value measured in ref 30 arises from the peptide NH group of Leu A722 and not the indole NH of Trp A697 as assigned in that study. Our calculations suggest that the presence of significant spin density on neighboring amino acid residues is facilitated solely by hydrogen bonding interactions with the semiquinone oxygen atoms. Similar hyperfine coupling values are calculated for the A_{1B} site; see below. A very recent HYSCORE study,[35] published while this paper was under review, found only one ^{14}N resonance which they assigned to the peptide N of Leu A722. The A_{iso} and anisotropic T values reported of 0.75−1.2 and 0.15−0.19 MHz are in good agreement with the values calculated in this study. In addition, the nuclear quadrupole coupling constant (NQCC) and asymmetry factor, η, reported are also in qualitative agreement with the calculated values shown in Table 4 for the Leu A722 peptide N.

Graphical Polar Plot Representation of Anisotropic Hyperfine Coupling Tensor. In Figure 4 we present a graphical representation of the anisotropic hyperfine coupling tensor as a polar plot for selected nuclei of model F. Such plots[36] are a highly useful means of graphically representing tensors in an intuitive way that indicates the orientation, sign, and relative magnitude of the principal components of the tensor with respect to the molecular frame.

For the Leu A722 peptide N interaction the principal positive value of 0.5 MHz (Table 4) corresponds to an axis direction closely aligned with the O4N direction. The tensor has axial symmetry (Figure 4a). For the C4 tensor (Figure 4b), we again have axial symmetry with the major positive component (27.6 MHz, Table 6) axis perpendicular to the PhSQ plane. A similar tensor symmetry can be expected for all other carbon and oxygen positions in the ring system. For the hydrogen bonding proton of the peptide NH of Leu A722 (Figure 4c), the major positive component (9.8 MHz) axis lies along the HO4 direction. As expected, axial symmetry is exhibited. For the H7 proton (Figure 4d), the major principal component axis lies along the CH bond direction with a value of 2.5 MHz (Table 5). The other principal directions are perpendicular to the CH bond in the ring plane, −1.9 MHz, and finally a much smaller magnitude component, −0.6 MHz, with an axis lying perpendicular to the PhSQ ring plane. A fuller account of this novel and informative representation of anisotropic hyperfine coupling tensors will be given in a future publication.

Table 7. ^{13}C Isotropic (A_{iso}) and Anisotropic (T_{nn}) Hyperfine Couplings Calculated for the A_{1A} and A_{1B} Sites[a]

	A_{1A}		A_{1B}	
	T_{11}	A_{iso}	T_{11}	A_{iso}
	T_{22}		T_{22}	
position	T_{33}		T_{33}	
C6	−1.6	−0.2	−1.7	0.1
	−1.4		−1.4	
	3.0		3.1	
C7	−3.1	2.3	−2.8	2.0
	−2.7		−2.4	
	5.8		5.1	
C8	−1.1	−3.8	−1.1	−3.8
	0.0		0.0	
	1.1		1.0	
C9	−4.9	−1.3	−3.6	−1.1
	−4.4		−3.0	
	9.4		6.6	
C10	−3.6	−5.0	−4.5	−4.7
	−3.0		−5.0	
	6.6		9.5	

[a] All values are given in MHz.

Table 8. ^{14}N and ^{17}O Isotropic (A_{iso}) and Anisotropic (T_{nn}) Hyperfine Couplings Calculated for the A_{1A} and A_{1B} Sites[a]

	A_{1A}			A_{1B}	
	T_{11}	A_{iso}	A_{11}	T_{11}	A_{iso}
	T_{22}		A_{22}	T_{22}	
position	T_{33}		A_{33}	T_{33}	
O1	33.2	−17.4	15.8	35.2	−17.5
	32.6		15.2	34.5	
	−65.8		−83.2 (84)	−69.7	
O4	31.8	−17.5	14.3	32.0	−17.3
	31.0		13.5	31.3	
	−62.8		−80.3 (77)	−63.3	
N (peptide NH) (Leu A722/Leu B706)	−0.2	1.4	1.2 (1.3)	−0.2	1.1
	−0.2		1.2 (1.3)	−0.2	
	0.5		1.9 (1.5)	0.4	

[a] The total (A_{nn}) values are also given for the N, O1, and O4 positions in the A_{1A} site, where they are compared with experimental magnitude determinations[23,30] given in parentheses. All values are given in MHz.

Comparison with Experimental and A_{1B} Site Values. In Tables 5, 6, 7, and 8, we report the complete hyperfine couplings calculated for both A_{1A} and A_{1B} sites for the largest model F. We also compare calculated ^{1}H, ^{13}C, and ^{17}O hyperfine couplings with the most recently experimentally reported values. We have already discussed this comparison for ^{17}O values. The ^{13}C and ^{1}H values are all in good agreement with experimentally reported values. As previously reported,[13,15] good agreement between experimental values and calculated values can be achieved using the smaller model B. As shown above, the principal modification to the spin density distribution in the extended models occurs mainly at the O1 and to a lesser extent at the C1 position, and hence the spin density at other positions is adequately accounted for by the smaller model B. While the ability of DFT calculations to quantitatively predict the largest ^{13}C A_{33} component of the C4 position has been criticized,[17] the value calculated in this study of 30.6 MHz (Table 5) is in reasonable agreement with the experimental value of 40 MHz. It should also be cautioned that the isotropic value for this position is liable to be difficult to calculate accurately. The isotropic value is a measure of the spin density at the nuclear position obtained from a Fermi contact analysis. Spin density at the C4 position arises due to spin polarization from the neighboring high spin density positions O4 and C2. This double contribution to the spin density at the C4 nucleus will cause the spin density at this nuclear[11]position and hence the associated isotropic hyperfine coupling constant to be less accurately calculated compared with positions where only one spin polarization pathway is dominant. Different experimental values have been reported in the literature for the hydrogen bonded proton of Leu A722. The experimental values given in Table 5 are the most recently reported in ref 15. Previous values in earlier reports[11,37]are in somewhat better agreement with our calculated values of this study. It should be pointed out that the inability to exchange the hydrogen bonded proton using D_2O leaves all of the experimental reports open to interpretation. The analysis of this portion of the ENDOR or TRIPLE spectrum is complicated by contributions from α protons on the PhSQ ring. Our calculations also show that significant ^{1}H anisotropic hyperfine couplings are found for the indole NH group of Trp A697 (2.3, −1.8, −0.5 MHz) and the α-CH group of Phe A689 (3.9, −1.8, −2.1 MHz) These need to be taken into account when interpreting experimental ENDOR or HYSCORE experimental data.

The hyperfine couplings for the A_{1B} site are also given in Tables 5−8, where they are compared with the A_{1A} site values. Values for the largest model F are given for both sites. While some small variations are noted, all values are very close to those obtained for the A_{1A} site, indicating an essentially identical spin density distribution for the PhSQ in both sites. There have been some ENDOR and TRIPLE resonance reports[38] which claim to have observed hyperfine couplings from the A_{1B} site PhSQ, and reported significant differences between values measured for the A_{1A} site. These claims have been questioned with the availability of more highly resolved ENDOR and TRIPLE data[15] which suggest that the data in ref 38 have been overinterpreted and possibly complicated by contamination from the A_0 chlorophyll radical. Our calculations suggest that the hyperfine couplings for the PhSQ radical in both sites should be very similar. It is notable that while the O4 anisotropic values are similar for both sites, the O1 major anisotropic coupling is calculated to be 4 MHz larger in magnitude for the A_{1B} site. Examination of the optimized structure around the O1 atom in both sites indicates that the interactions of this atom with the Trp B677 indole NH and particularly the Phe B669 α-CH fragment are smaller in the A_{1B} site compared with the A_{1A} site. As described above, the equivalent fragments in the A_{1A} site principally contribute to a lowering in the magnitude of the O1 principal value for PhSQ. This reduced interaction for the A_{1B} site quinone will reduce the electron affinity of the quinone sited there compared with the A_{1A} site and is in qualitative agreement with the stronger reducing ability reported for the A_{1B} quinone.[4,35] Further, more detailed calculations on this topic are needed and are currently underway.

CONCLUSIONS

Using DFT-based electronic structure calculations, we have shown that while the O1 atom of the PhSQ in the A_{1A} site of PS I is not involved in direct hydrogen bonding, the ^{17}O anisotropic hyperfine coupling for this position is sensitive to interactions with neighboring groups, especially Trp A697 and Phe A689. The results obtained are in agreement with experimental determinations which indicate small differences in ^{17}O hyperfine couplings for both oxygen atoms.[23] Good agreement between calculated and experimental ^{1}H and ^{13}C hyperfine couplings is also found. In addition, for extended site models, we have found that a significant ^{14}N isotropic coupling is calculated for the peptide NH group of Leu A722. The ^{14}N isotropic hyperfine coupling obtained for the indole nitrogen atom of Trp A697 is calculated to be zero, calling into question a previous experimental assignment. The spin density distribution of the PhSQ in the A_{1B} site is calculated to be similar to that in the A_{1A} site. On the basis of the calculated perturbation of the spin density of the primary acceptor semiquinone, we conclude that the number of hydrogen bonds to the semiquinone is lower, and the strength of the hydrogen bonds is weaker, in the PS I reaction center compared with type II reaction centers. This reduced hydrogen bonding activity will contribute substantially to the significantly lower redox potential of the PS I quinone compared with the type II quinone.

ASSOCIATED CONTENT

Supporting Information. A_{1A} site model optimized coordinates in Protein Data Bank (PDB) format and A_{1B} site model optimized coordinates in PDB format. This material is available free of charge via the Internet at http://pubs.acs.org.

AUTHOR INFORMATION

Corresponding Author

*E-mail: patrick.omalley@manchester.ac.uk. Phone/fax: 0041612004536.

ACKNOWLEDGMENT

We acknowledge the use of the EPSRC UK National Service for Computational Chemistry Software (NSCCS) in carrying out this work.

ABBREVIATIONS USED

DFT, density functional theory; B3LYP, Becke3 Lee−Yang−Parr; QM, quantum mechanics; MM, molecular mechanics; PhQ, phylloquinone; PhSQ, phyllosemiquinone; PS II, photosystem II; PS I, photosystem I; RC, reaction center; ONIOM, our own *N*-layered integrated molecular orbital and molecular mechanics; EPR, electron paramagnetic resonance; ENDOR, electron nuclear double resonance; ESEEM, electron spin echo envelope modulation; HYSCORE, hyperfine sublevel correlation spectroscopy

REFERENCES

(1) Blankenship, R. E. *Molecular Mechanisms of Photosynthesis*, 1st ed.; Blackwell Science: Oxford, U.K., 2002.

(2) Jordan, P.; Fromme, P.; Witt, H. T.; Klukas, O.; Saenger, W.; Krauss, N. *Nature* **2001**, *411*, 909.

(3) Holzwarth, A. R.; Muller, M. G.; Niklas, J.; Lubitz, W. *Biophys. J.* **2006**, *90*, 552.

(4) Srinivasan, N.; Golbeck, J. H. *Biochim. Biophys. Acta, Bioenerg.* **2009**, *1787*, 1057.

(5) Muller, M. G.; Slavov, C.; Luthra, R.; Redding, K. E.; Holzwarth, A. R. *Proc. Natl. Acad. Sci. U.S.A.* **2010**, *107*, 4123.

(6) Santabarbara, S.; Reifschneider, K.; Jasaitis, A.; Gu, F. F.; Agostini, G.; Carbonera, D.; Rappaport, F.; Redding, K. E. *J. Phys. Chem. B* **2010**, *114*, 9300.

(7) Lubitz, W.; Feher, G. *Appl. Magn. Reson.* **1999**, *17*, 1.

(8) O'Malley, P. J. *Chem. Phys. Lett.* **1996**, *262*, 797.

(9) Lin, T. J.; O'Malley, P. J. *THEOCHEM* **2008**, *870*, 31.

(10) Heathcote, P.; MoenneLoccoz, P.; Rigby, S. E. J.; Evans, M. C. W. *Biochemistry* **1996**, *35*, 6644.

(11) Rigby, S. E. J.; Evans, M. C. W.; Heathcote, P. *Biochemistry* **1996**, *35*, 6651.

(12) Kamlowski, A.; Altenberg-Greulich, B.; van der Est, A.; Zech, S. G.; Bittl, R.; Fromme, P.; Lubitz, W.; Stehlik, D. *J. Phys. Chem. B* **1998**, *102*, 8278.

(13) O'Malley, P. J. *Biochim. Biophys. Acta, Bioenerg.* **1999**, *1411*, 101.

(14) Teutloff, C.; Bittl, R.; Lubitz, W. *Appl. Magn. Reson.* **2004**, *26*, 5.

(15) Niklas, J.; Epel, B.; Antonkine, M. L.; Sinnecker, S.; Pandelia, M. E.; Lubitz, W. *J. Phys. Chem. B* **2009**, *113*, 10367.

(16) Sakuragi, Y.; Zybailov, B.; Shen, G. Z.; Bryant, D. A.; Golbeck, J. H.; Diner, B. A.; Karygina, I.; Pushkar, Y.; Stehlik, D. *J. Biol. Chem.* **2005**, *280*, 12371.

(17) Karyagina, I.; Golbeck, J. H.; Srinivasan, N.; Stehlik, D.; Zimmermann, H. *Appl. Magn. Reson.* **2006**, *30*, 287.

(18) Teutloff, C.; Hofbauer, W.; Zech, S. G.; Stein, M.; Bittl, R.; Lubitz, W. *Appl. Magn. Reson.* **2001**, *21*, 363.

(19) Semenov, A. Y.; Vassiliev, I. R.; van der Est, A.; Mamedov, M. D.; Zybailov, B.; Shen, G. Z.; Stehlik, D.; Diner, B. A.; Chitnis, P. R.; Golbeck, J. H. *J. Biol. Chem.* **2000**, *275*, 23429.

(20) Feldman, K. S.; Hester, D. K.; Golbeck, J. H. *Bioorg. Med. Chem. Lett.* **2007**, *17*, 4891.

(21) O'Malley, P. J. *Chem. Phys. Lett.* **1997**, *274*, 251.

(22) Vreven, T.; Byun, K. S.; Komaromi, I.; Dapprich, S.; Montgomery, J. A.; Morokuma, K.; Frisch, M. J. *J.Chem. Theory Comput.* **2006**, *2*, 815.

(23) Pushkar, Y. N.; Ayzatulin, O.; Stehlik, D. *Appl. Magn. Reson.* **2005**, *28*, 195.

(24) Frisch, M. J.; Trucks, G. W.; Schlegel, H. B.; Scuseria, G. E.; Robb, M. A.; Cheeseman, J. R.; Montgomery, J. A., Jr.; Vreven, T.; Kudin, K. N.; Burant, J. C.; Millam, J. M.; Iyengar, S. S.; Tomasi, J.; Barone, V.; Mennucci, B.; Cossi, M.; Scalmani, G.; Rega, N.; Petersson, G. A.; Nakatsuji, H.; Hada, M.; Ehara, M.; Toyota, K.; Fukuda, R.; Hasegawa, J.; Ishida, M.; Nakajima, T.; Honda, Y.; Kitao, O.; Nakai, H.; Klene, M.; Li, X.; Knox, J. E.; Hratchian, H. P.; Cross, J. B.; Adamo, C.; Jaramillo, J.; Gomperts, R.; Stratmann, R. E.; Yazyev, O.; Austin, A. J.; Cammi, R.; Pomelli, C.; Ochterski, J. W.; Ayala, P. Y.; Morokuma, K.; Voth, G. A.; Salvador, P.; Dannenberg, J. J.; Zakrzewski, V. G.; Dapprich, S.; Daniels, A. D.; Strain, M. C.; Farkas, O.; Malick, D. K.; Rabuck, A. D.; Raghavachari, K.; Foresman, J. B.; Ortiz, J. V.; Cui, Q.; Baboul, A. G.; Clifford, S.; Cioslowski, J.; Stefanov, B. B.; Liu, G.; Liashenko, A.; Piskorz, P.; Komaromi, I.; Martin, R. L.; Fox, D. J.; Keith, T.; Al-Laham, M. A.; Peng, C. Y.; Nanayakkara, A.; Challacombe, M.; Gill, P. M. W.; Johnson, B.; Chen, W.; Wong, M. W.; Gonzalez, C.; Pople, J. A. *Gaussian 09*; Gaussian, Inc.: Wallingford, CT, USA, 2009.

(25) O'Malley, P. J. *J. Phys. Chem. A* **1997**, *101*, 6334.

(26) Heathcote, P.; Rigby, S. E. J.; Evans, M. C. W. *Photosynthesis: From Light to Biosphere*; Springer: New York; 1995; Vol. II, p 163.

(27) Xu, W.; Chitnis, P. R.; Valieva, A.; van der Est, A.; Brettel, K.; Guergova-Kuras, M.; Pushkar, Y. N.; Zech, S. G.; Stehlik, D.; Shen, G. Z.; Zybailov, B.; Golbeck, J. H. *J. Biol. Chem.* **2003**, *278*, 27876.

(28) Deligiannakis, Y.; Hanley, J.; Ruthesford, A. W. *J. Am. Chem. Soc.* **1999**, *121*, 7653.

(29) Chatterjee, R.; Milikisiyants, S.; Coates, C. S.; Lakshmi, K. V. *Biochemistry* **2011**, *50*, 491.

(30) Hanley, J.; Deligiannakis, Y.; MacMillan, F.; Bottin, H.; Rutherford, A. W. *Biochemistry* **1997**, *36*, 11543.

(31) Deligiannakis, Y.; Boussac, A.; Rutherford, A. W. *Biochemistry* **1995**, *34*, 16030.
(32) Spoyalov, A. P.; Hulsebosch, R. J.; Shochat, S.; Gast, P.; Hoff, A. J. *Chem. Phys. Lett.* **1996**, *263*, 715.
(33) Martin, E.; Narasimhulu, K. V.; Samoilova, R. I.; Lin, T. J.; Wraight, C. A.; O'Malley, P. J.; Dikanov, S. A. *J. Am. Chem. Soc.* **2011**, *133*, 5526.
(34) Astashkin, A. V.; Kawamori, A.; Kodera, Y.; Kuroiwa, S.; Akabori, K. *J. Chem. Phys.* **1995**, *102*, 5583.
(35) Srinivasan, N.; Chatterjee, R.; Milikisiyants, S.; Golbeck, J. H.; Lakshmi, K. V. *Biochemistry* **2011**, *50*, 3495.
(36) Autschbach, J.; Zheng, S. H.; Schurko, R. W. *Concepts Magn. Reson., Part A* **2010**, *36A*, 84.
(37) Stehlik, D.; Karyagina, I.; Golbeck, J. *Photosynth. Res.* **2007**, *91*, 140.
(38) Rigby, S. E. J.; Muhiuddin, I. P.; Evans, M. C. W.; Purton, S.; Heathcote, P. *Biochim. Biophys. Acta, Bioenerg.* **2002**, *1556*, 13.